George V. Waldo, Jr.
Naval Surface Warfare Center
Carderock Division
Bethesda, MD 20084-5000

Reflected-Afterflow Virtual-Source Model Compared to Exact Calculations for Elastic Cylinders Attacked by Planar Waves

A recently developed theoretical approximation, the reflected-afterflow virtual-source (RAVS) model, is applied to the case of a planar shock wave attacking an elastic cylindrical shell. Calculations are shown to be in good agreement with the exact calculations that were published by Huang for all locations and times. It is concluded that the RAVS model gives a good approximation for the loading and response of an elastic cylindrical shell attacked by planar waves. The RAVS model is shown to be even better for spherical waves that are of much more practical interest. © *1997 John Wiley & Sons, Inc.*

INTRODUCTION

Calculation of the deformation of a structure caused by the pressure wave from an underwater explosion is of much interest to the Navy. To gain this capability an approximate model was introduced (Waldo, 1994) to determine the pressure that develops when an acoustic wave interacts with a curved and compliant surface. This model uses the virtual-source concept in analogy with geometrical optics. Because this model includes the afterflow velocities of both the attacking and reflected waves, it is called the reflected-afterflow virtual-source (RAVS) model. In this article an equation of motion for a structural surface is obtained using the RAVS model. From this equation of motion, the deformation of the surface is calculated. A procedure is presented to determine the deformations for the special case of a planar shock wave interacting with a cylindrical elastic cell. Calculations with this procedure, using RAVS, are shown to be in good agreement with the exact calculations by Huang (1970).

EQUATION OF MOTION

The equation of motion for the velocity $u(t)$ of the surface in the direction that is *opposite* to the normal to the surface (Fig. 1) is

Received February 28, 1996; Accepted September 9, 1996
Shock and Vibration, Vol. 4, No. 2, pp. 93–102 (1997)
© 1997 by John Wiley & Sons, Inc.
CCC 1070-9622/97/020093-10

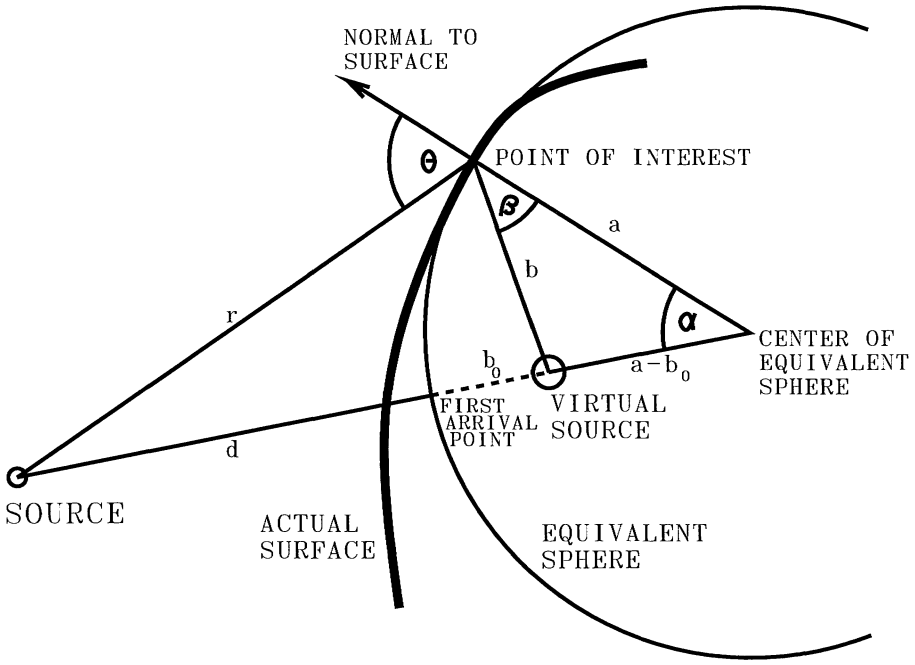

FIGURE 1 Geometry for virtual source.

$$m\dot{u}(t) = p_{tot}(t) - p_{str}(t), \tag{1}$$

where m is the total mass (including the attached stiffeners) of the structural surface per unit area, t is the time after arrival of the attacking wave, $p_{tot}(t)$ is the total pressure in the fluid, and $p_{str}(t)$ is the structural pressure, i.e., the force per unit area due to the structure in the direction that is normal to the structural surface (pointing into the fluid). This quantity is determined by the properties of the structure. The total pressure in the fluid at the point of interest on the surface of the structure is

$$p_{tot}(t) = p_{hydro} + p(t) + p_{scat}(t) + p_{rad}(t), \tag{2}$$

where p_{hydro} is the hydrostatic pressure, $p(t)$ is the pressure of the attacking wave, $p_{scat}(t)$ is the pressure of the scattered wave, and $p_{rad}(t)$ is the pressure of the radiated wave. To determine these pressures, it is necessary to review the derivations in an earlier study (Waldo, 1994):

AFTERFLOW

The velocity of the fluid for a spherical acoustic wave can be expressed as

$$v(t) = \frac{p(t)}{\rho c} + \frac{1}{\rho r}\int_0^t p(t')\,dt', \tag{3}$$

where ρ is the mass density of the fluid, c is the speed of sound, and r is the distance from the source. The second term in this equation (with the integral) is called the afterflow term (see, e.g., Cole, 1948, p. 143).

SCATTERED WAVE AND RADIATED WAVE

When the acoustic wave interacts with the surface of a structure, an additional pressure is developed at the surface. If there is no separation between the fluid and the surface, then the velocity of the fluid in the direction that is normal to the surface must equal the velocity of the surface in the direction that is normal to the surface. The total pressure of the fluid is equal to the sum of the hydrostatic pressure, the pressure of the incident wave, and the additional pressure that arises from the interaction with the surface. This additional pressure is modeled as the superposition of a "scattered" wave and a "radiated" wave. The scattered wave is defined to be the wave that would occur if the surface did not move (if there were no separation of the fluid from the surface). The radiated

wave is defined to be the remainder of the additional pressure wave and is the result of the movement of the surface (if there were no separation of the fluid from the surface).

Scattered Wave

The pressure due to the scattered wave at a point on the surface is determined by modeling the scattered wave as if it emanated from a "virtual" source analogous with geometrical optics. For this model, consider a point of interest on the surface of the structure that is at a distance r from the source (Fig. 1). The surface at this point is modeled as an "equivalent" sphere with radius a that is determined by

$$\frac{1}{a} = \frac{1}{2}\left(\frac{1}{a_1} + \frac{1}{a_2}\right), \tag{4}$$

where a_1 is the radius of curvature in a given direction on the actual surface and a_2 is the radius of curvature in the direction that is perpendicular to the given direction. Of course, a complicated surface with sharp angles would have to be smoothed by an algorithm or engineering judgment. For example, if the surface is attacked by a positive pressure pulse, then the smoothing could be over the length of the pulse, if the pulse length is smaller than the characteristic dimension of the object. If the pulse were longer, then the smoothing could be over the characteristic dimension of the object. However, for a simple surface, it can be easily shown that the radius of this equivalent sphere does not vary on the given direction of a_1. If the actual surface were a sphere, then $a_1 = a_2 = a$. However, if the actual surface were a cylinder, then a_2 is infinite and $a = 2a_1$. The surface of the equivalent sphere is superposed on the actual surface at the point of interest. The radial direction of the equivalent sphere is the same as the normal direction to the actual surface at the point of interest.

The geometry of the source and the point of interest is also shown in Fig. 1. The distance from the source to the equivalent sphere and an associated angle about the center of the equivalent sphere are determined as follows: consider the line from the source to the center of this equivalent sphere. Define d to be the distance along this line from the source to the surface of the equivalent sphere. The intersection of this line with the equivalent sphere is the point on the equivalent sphere that is closest to the source. This is called "the first arrival point." At the point of interest (see Fig. 1), the angle of incidence θ is the angle between the normal to the surface and the line from the source. Thus,

$$d = \frac{r^2 + 2ra\cos\theta}{\sqrt{r^2 + a^2 + 2ra\cos\theta} + a}. \tag{5}$$

The angle α between the line from the source to the center of the equivalent sphere and the line from the center of the sphere to the point of interest is determined from Fig. 1 to be

$$\begin{aligned} \alpha &= \zeta, && \text{for } a + r\cos\theta \geq 0, \\ \alpha &= \zeta + \pi, && \text{for } a + r\cos\theta < 0, \end{aligned} \tag{6}$$

where

$$\zeta = \arctan\left(\frac{r\sin\theta}{a + r\cos\theta}\right). \tag{7}$$

As in geometrical optics, the scattered wave is modeled as emanating from a virtual source. The distance b_0 from the surface of the equivalent sphere to this virtual source is given by

$$\frac{1}{b_0} = \frac{1}{d} + \frac{2}{a}, \quad \text{for } d > 0 \text{ and } a > 0, \tag{8}$$

(see, e.g., Jenkins and White, 1957, p. 87). This concept is valid only for early times ($ct \ll a$ or oscillatory waves with wavelengths $\ll a$) and for points on the equivalent sphere that are near the first arrival point. However, it is *assumed* in this model that this is approximately correct even if the points are not near the first arrival point. Of course, if the actual surface is not a sphere, then it is *assumed* that this equivalent spherical model is approximately correct.

In the case with $d \leq 0$, the virtual source is assumed to be located at the actual source. This implies that $b = r$ and $\beta = \pi - \theta$ (see Fig. 1). Under certain conditions, a calculation might be acceptable for a concave surface [i.e., a surface with an equivalent sphere having a negative radius Eq. (4)]. However, there are complications that could occur for other conditions. Thus, for the models that are presented in this article, it is required that $a > 0$. For numerical calculations, if a were negative, then it would have to be set equal to a very large positive number so that the effective

curvature in the calculation would be approximately zero.

It is emphasized that if the actual surface is not a sphere, then there is a *different* virtual source for *each* point of interest on the structural surface. Thus, for the acoustic radiation into the entire fluid, this model is only an approximate solution to the wave equation. For points on the equivalent sphere that are near the first arrival point, these virtual sources are very close together so that their effect is approximately the same as a single virtual source. Of course, the validity of this model must be tested by comparison with problems for which exact solutions are available.

The geometry about the virtual source is also shown in Fig. 1. The distance from the virtual source to the point of interest and the angle of the scattered wave are determined as follows: from Fig. 1 it can be seen that the distance from the virtual source to the point of interest is

$$b = \sqrt{b_0^2 + 4a(a - b_0)\,[\sin(\alpha/2)]^2}. \tag{9}$$

Also, Fig. 1 shows that the angle of the scattered wave β between the radial direction and the line to the virtual source can be determined from

$$\cos\beta = \{b_0 + 2(a - b_0)[\sin(\alpha/2)]^2\}/b, \tag{10}$$

which is positive for $a > 0$ and $d > 0$; see Eq. (8) for b_0, Eq. (6) for α, and Eq. (9) for b.

The velocity of the fluid due to the scattered wave is

$$v_{\text{scat}}(t) = \frac{p_{\text{scat}}(t)}{\rho c} + \frac{1}{\rho b}\int_0^t p_{\text{scat}}(t')\,dt', \tag{11}$$

where $p_{\text{scat}}(t)$ is the pressure of the scattered wave [see Eq. (3)].

Because the scattered wave is defined to be the wave that would occur if the surface did not move (if there were no separation of the fluid from the surface), the velocity of the fluid in the direction of the normal to the surface must be zero. That is,

$$v(t)\cos\theta - v_{\text{scat}}(t)\cos\beta = 0. \tag{12}$$

Substituting Eq. (11) in Eq. (12) and differentiating with respect to t gives

$$\frac{\dot{p}_{\text{scat}}(t)}{\rho c} + \frac{p_{\text{scat}}(t)}{\rho b} = \dot{v}(t)\frac{\cos\theta}{\cos\beta}. \tag{13}$$

Solving this equation, substituting Eq. (3) [for $v(t)$] in the resulting equation, and integrating by parts gives the pressure of the scattered wave,

$$p_{\text{scat}}(t) = \left[p(t) - c\left(\frac{1}{b} - \frac{1}{r}\right)e^{-(ct/b)} \int_0^t e^{ct'/b}\,p(t')\,dt'\right]\frac{\cos\theta}{\cos\beta}. \tag{14}$$

Pressure of Radiated Wave

The pressure at the point of interest due to the radiated wave is also modeled as if it were emanating from the virtual source. This pressure is determined by solving

$$u(t) = -\left[\frac{p_{\text{rad}}(t)}{\rho c} + \frac{1}{\rho b}\int_{-r/c}^t p_{\text{rad}}(t')\,dt'\right]\cos\beta, \tag{15}$$

where $u(t)$ is the velocity of the surface in the direction that is *opposite to* the normal to the surface, i.e., the velocity in the direction *into* the surface of the structure. The lower limit of the integral in this equation is $-r/c$, rather than zero, because movement in the structure might propagate faster than in the fluid. (Note that the opposite sign convention is used by Huang, 1970.) Thus, as in eq. (22) of Waldo (1994), the pressure of the radiated wave is

$$p_{\text{rad}}(t) = -e^{-(ct/b)}\int_{-r/c}^t e^{ct'/b}\frac{\rho c\dot{u}(t')}{\cos\beta}\,dt'. \tag{16}$$

Of course, it is *assumed* that the deformations of the surface are so small that they have a negligible effect on the curvatures. If these curvatures were continually updated during a calculation to give the current curvature, there would be an improvement in the calculation.

Equations Applied to All Points

It must be emphasized that all of these equations are applied to all points on the surface of the structure being attacked. This includes points that are in the shadow of the structure with respect to the source.

SOLUTION OF EQUATION OF MOTION

The solution of Eq. (1) is presented in the Appendix [see Eq. A.13)]. To perform numerical calcula-

tions with this solution, the increment of $I(t)$ [see Eqs. (A.3) and (A.5)] is

$$\begin{aligned}\Delta I &= I(t+\Delta t) - I(t) = e^{-\eta(t+\Delta t)} \int_t^{t+\Delta t} e^{\eta t'} p(t')\, dt' \\ &\quad - (1 - e^{-\eta \Delta t})\, I(t) \\ &\approx e^{-\eta(t+\Delta t)} \frac{e^{\eta(t+\Delta t)} - e^{\eta t}}{\eta} p(t+\Delta t) \\ &\quad - (1 - e^{-\eta \Delta t}) I(t) \\ &= [p(t+\Delta t) - \eta I(t)] Q,\end{aligned} \tag{17}$$

where

$$\begin{aligned}Q &= \frac{1 - e^{-\eta \Delta t}}{\eta} \\ &= \frac{2}{\eta} \exp\left(-\frac{\eta}{2}\Delta t\right) \sinh\left(\frac{\eta}{2}\Delta t\right).\end{aligned} \tag{18}$$

This would be exact if $p(t)$ were constant in the interval $(t, t + \Delta t]$. (This interval must include $t + \Delta t$ because p is defined at $t + \Delta t$.) Note that $I(t) = 0$ for $t \leq 0$. The numerical calculation of $I_{str}(t)$ [see Eq. (A.4)] can be performed in a similar fashion.

PLANAR ATTACKING WAVE

For a planar attacking wave, the source is at an infinite distance. In this case, $r \to \infty$, which implies that $d \to \infty$ [see Eq. (5)]. Thus, it is seen from Eq. (8) that $b_0 \to a/2$ and from Eq. (6) that $\alpha \to \theta$.

For a cylindrical surface, a_2 is infinite. Thus, for a planar wave propagating perpendicular to the axes of the cylinder, $a = 2a_1$ and $b_0 = a_1$ [see Eqs. (4), (8)]. Also, the angle of incidence, θ, is the same as the angle of the point of interest on the cylinder above the direction of propagation of the wave, as shown in Fig. 2.

For a cylindrical shell (see Fig. 2) composed of elastic material with Young's modulus E, Poisson's ratio ν, thickness $2h$, and radius a_1, my earlier study shows (Waldo 1996) that the structural resistance pressure, used by Huang (1970), is equivalent to

$$\begin{aligned}p_{str} &= \frac{2Eh}{(1-\nu^2)a_1^2} \\ &\quad \left[d_{radial} + \frac{h^2}{3a_1^2} d^{(4)}_{radial} - d^{(1)}_{\theta} + \frac{h^2}{3a_1^2} d^{(3)}_{\theta}\right],\end{aligned} \tag{19}$$

where d_{radial} is the deflection in the radial direction

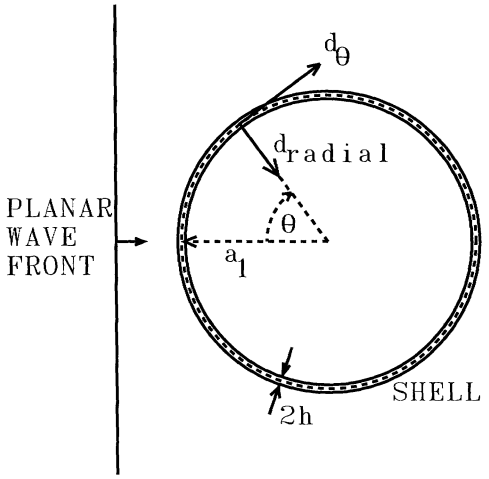

FIGURE 2 Planar wave attacking a cylindrical shell.

and d_θ is the deflection in the tangential direction. My study also showed (Waldo, 1996) that the equation of motion for the tangential deflection is equivalent to

$$\begin{aligned}\ddot{d}_\theta &= \frac{1}{m} \frac{2Eh}{(1-\nu^2)a_1^2} \\ &\quad \left[\left(1 + \frac{h^2}{3a_1^2}\right) d^{(2)}_{\theta} - d^{(1)}_{radial} + \frac{h^2}{3a_1^2} d^{(3)}_{radial}\right],\end{aligned} \tag{20}$$

where $m = 2\rho_s h$ in which ρ_s is the mass density of the shell material. A computer program using these equations is presented in the same study (Waldo, 1996).

Comparisons to Exact Calculations

Exact calculations for this problem were performed by Huang (1970). Equation (1) of Huang's article states that

$$M = \rho a_1/(2h\rho_s) \quad \text{and} \quad C^2 = E/[\rho_s(1-\nu^2)c^2]. \tag{21}$$

His results for these dimensionless quantities can be regarded as functions of the number of radial transit times after arrival of the front of the attacking wave at $\theta = 0$, i.e., $T^* = cT/a_1$, where T is the time after arrival of the attacking wave at $\theta = 0$. [Thus, the time after arrival of the front at a given location is $t = T - (1 - \cos\theta)a_1/c$.] In a similar fashion, the nondimensional radial velocity is defined as $u^* = u\rho c/p_0$. Also, for a time-decay

constant q, the attacking pressure is $p(t) = p_0 e^{-t/q}$, for $t > 0$ and is zero otherwise.

Situation with $M = 2$, $h/a_1 = 1/31$, and $C^2 = 13.685665$

The situation with $M = 2$, $h/a_1 = 1/31$, and $C^2 = 13.685665$ was treated for $q = 0$. Figure 3 shows the comparison of the RAVS calculation with Huang's (1970) exact calculation for this case. Note that the curves are very close even though the minima of the oscillations in the RAVS calculation are slightly lower than those in Huang's calculation.

Because Huang's (1970) exact calculation contains only eight modes, it is not quite exact. However, because the convergence is very rapid, there is little error in Huang's calculation. Also, because his curves were read directly from his journal article, there are some small errors in the presentation of his curves in this article. As can be seen in my finite-difference program (Waldo, 1996), the calculation with the RAVS model had 12 space intervals for $\theta = 0$ to $\theta = \pi$. For twice this number of intervals, the calculation was about the same. Thus, the calculation is sufficiently accurate for this comparison.

The zeroth mode of the radial displacement [see eq. (5) of Huang, 1970] is defined as

$$d_{\text{radial0}}(t) = \frac{1}{\pi}\int_0^{\pi} d_{\text{radial}}(t, \theta)\, d\theta. \qquad (22)$$

The nondimensional form of this quantity, $d^*_{\text{radial0}} = (d_{\text{radial0}}/a_1)\rho c^2/p_0$, is plotted in Waldo (1996). Again, the curves are so close that they overlap and are not discernible. Also, the RAVS calculation at 10 radial transit times, 0.1458, is almost the same as the exact asymptotic value $M/C^2 = 0.1461$ (see Huang, 1970).

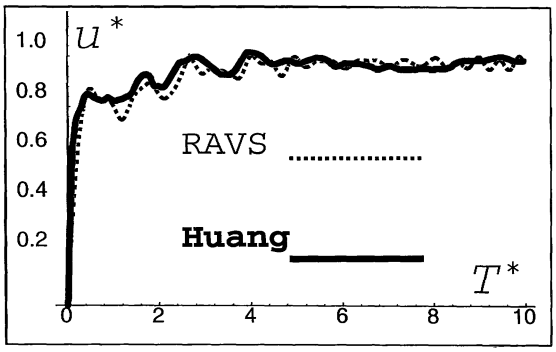

FIGURE 3 Nondimensional velocity vs. time, $\theta = 0$, $q = 0$, $M = 2$.

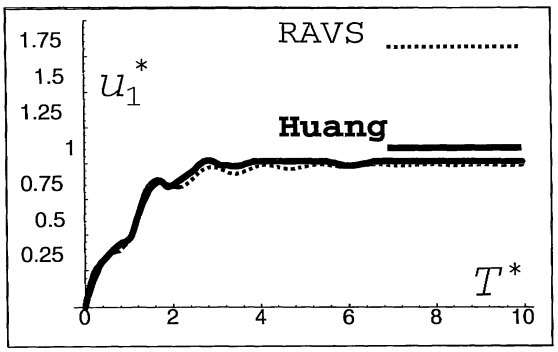

FIGURE 4 Nondimensional velocity vs. time, first mode, $q = 0$, $M = 2$.

The first mode of the radial velocity [see eq. (5) of Huang, 1970] is defined as

$$u_1(t) = \frac{2}{\pi}\int_0^{\pi} u(t, \theta)\cos\theta\, d\theta. \qquad (23)$$

The nondimensional form of this quantity, $u^* = u_1\rho c/p_0$, is plotted in Fig. 4. As above, the curves are very close.

Situation with $M = 4.41890$, $h/a_1 = 1/69$, and $C^2 = 12.581197$

The situation with $M = 4.41890$, $h/a_1 = 1/69$, and $C^2 = 12.581197$ was also treated for $q = 0$. For $\theta = 0$ in Fig. 5 the agreement between the RAVS and the exact solution is very good. In particular, the first two (most important) oscillations are reproduced by the RAVS calculation with very little

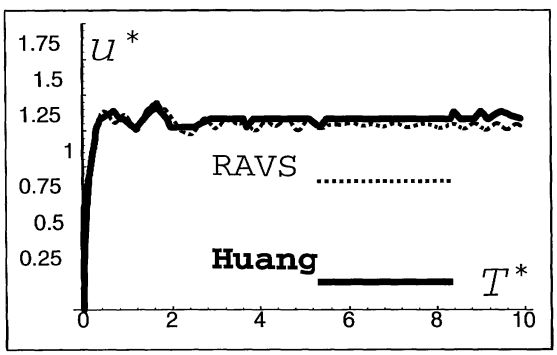

FIGURE 5 Nondimensional velocity vs. time, $\theta = 0$, $q = 0$, $M = 4.4189$.

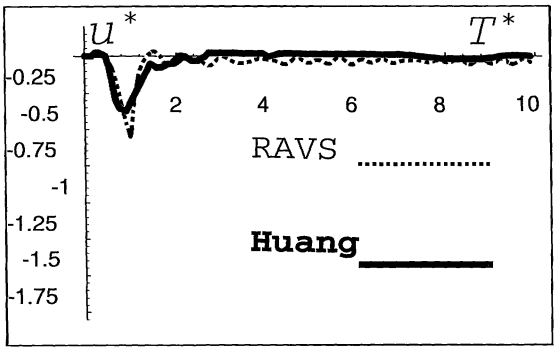

FIGURE 6 Nondimensional velocity vs. time, $\theta = \pi/2$, $q = 0$, $M = 4.4189$.

error. The agreement at $\theta = \pi/2$ in Fig. 6 is also very good. Because Huang only had a finite number of modes in his calculation, there is a small precursor due to the Gibbs phenomena (as discussed by Huang, 1970). Thus, because of the Gibbs phenomena, the true (exact) minimum value in Fig. 6 might be even closer to the RAVS calculation. Of course, this conjecture would have to be verified by including many more modes in Huang's calculation. The agreement at $\theta = \pi$ (at the back of the cylinder, see Waldo, 1996), is very good up to two radial transit times. For later times the RAVS velocity is a fairly good approximation of the exact velocity, even though it is somewhat lower. However, for many practical situations, the front side is of greatest interest. For these situations, the calculation for the back of the cylinder does not need to be very accurate if it is not too large. Also, in many practical situations, the cylinder contains enough internal equipment so that the entire object is neutrally buoyant. Often, after two radial transit times, this internal equipment will attain velocities that are close to the velocity of the shell. That is, the entire object will be moving almost as if it were a neutrally buoyant shell such as treated in Figs. 3 and 4. Thus, if the entire object (including internal equipment) were modeled using the RAVS model, then it is plausible that the motions would be close to those of the neutrally buoyant shell for which the agreement is very good with the exact calculations. That is, in these practical situations, the RAVS calculation might be close to the exact motion even on the back of the shell.

The exact calculations of the strains for this situation (Fig. 7) are in very good agreement with the RAVS calculations for all times and all locations (also see Waldo, 1996). Note that in this figure, the ordinate is defined as the strain multiplied by a nondimensional factor, i.e.,

$$\text{strain}^* = \text{strain}\ \rho c^2/p_0, \tag{24}$$

where strain $= (d_\theta^{(1)} - d_{\text{radial}})/a_1$. It is seen that the most important oscillatory behavior is accurately replicated by the RAVS calculation. Even though the *velocity* (shown in Waldo, 1996) at $\theta = \pi$ was somewhat smaller than the exact calculation after two radial transit times, the *strain* (Fig. 7) at this location is almost the same as the exact calculation. This is significant because the strains are a better measure of the condition of the shell than the velocity. Note that the small-amplitude and high-frequency oscillations are due to using only 48 intervals from $\theta = 0$ to $\theta = \pi$ in the finite-difference program, (see Waldo, 1996). If more intervals were used, then these amplitudes would be even smaller and these frequencies would be even higher. This would make the agreement with the exact calculation even better. Also note that all of the calculations have only 12 intervals except the strain calculations (see Fig. 7, which has 48 intervals).

The zeroth mode for the radial displacement, Eq. (22), is shown in Waldo (1996). Again the agreement is very good. At 10 radial transit times, the RAVS calculation is 0.35111, which is almost the same as the exact asymptotic value (Huang, 1970) $M/C^2 = 0.35123$. As expected, the zeroth mode of displacement is almost the same as the values of strain for this time.

The exact values of the first mode for velocity (see Waldo, 1996) are almost the same as the values calculated using the RAVS model up to two radial transit times. For later times, the RAVS model gives a good approximation, even though the values are somewhat lower. These lower values

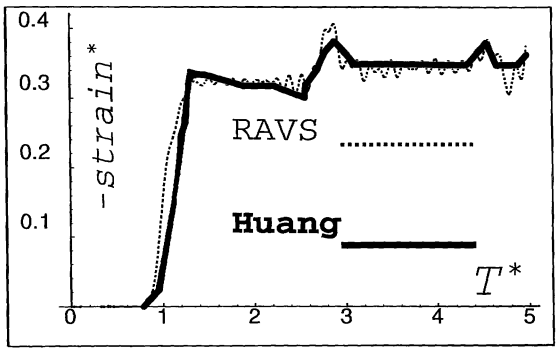

FIGURE 7 Strain vs. nondimensional time, $\theta = \pi$, $q = 0$, $M = 4.4189$.

are due to the lower values of velocity at the back of the cylinder.

Situation with $M = 6.41975$, $h/a_1 = 1/100$, $C^2 = 13.685665$, and $q = 0$

The situation with $M = 6.41975$, $h/a_1 = 1/100$, $C^2 = 13.685665$, and $q = 0$ is compared for the zeroth displacement mode in Waldo (1996). Even though the RAVS calculation rises somewhat faster than the exact calculation, the agreement is very good. The value for 10 radial transit times is 0.46909, which is the same as the exact asymptotic value (Huang, 1970) $M/C^2 = 0.46909$, to five significant figures. The RAVS calculation of the first velocity mode (Waldo, 1996) agrees very well up to two radial transit times. At later times, it is a fair approximation even though it is lower than the exact values. Unfortunately, Huang (1970) did not present the calculations for the velocities and strains at individual locations for this situation. As explained above, for many situations of interest with internal equipment inside the shell, the velocities at later times would tend to be the same as in the neutrally buoyant situation. For the neutrally buoyant situation, the RAVS calculation agrees very well with the exact calculation. Thus, the small deviation after two radial transit times might be of little practical interest. In addition, in the previous situation the velocities on the front of the cylinder and the strains at all locations were very close to the exact calculations, even though the zeroth velocity mode was somewhat lower than the exact calculation after two radial transit times. Thus, it is plausible that the velocities on the front of the cylinder and the strains at all locations are in better agreement than the first velocity mode.

Other Situations Published by Huang

The other situations that were published by Huang (1970), including those with $q > 0$, agreed about as well with the RAVS calculation as the cases presented above (see Waldo, 1995, 1996) for all of the comparisons).

RIGID CYLINDERS

My previous study showed (Waldo, 1994) that the RAVS calculations for *rigid* (*and immovable*) cylinders attacked by plane waves are in good agreement with the exact calculations. However, the preceding calculations for elastic cylinders attacked by planar waves are in even better agreement with the exact calculations. Also in Waldo (1994), RAVS calculations are compared to Huang's (1975) exact calculations for a *spherical* wave from a source that is 0.5 from the nearest point on the cylinder [see Eq. (2), with $p_{\text{hydro}} = p_{\text{rad}} = 0$, $a_1 = 1$, and $c = 1$] and has a step pressure $p(t) = 0.5/r$, for $0 \leq t$ (see Fig. 8). It is seen that the error for 0° is very small. The exact pressures at 90°, 120°, and 180° are so much smaller than that at 0°, that for many purposes they can be disregarded (at these angles, the RAVS calculations give zero pressure). Because the RAVS calculations for the elastic case are in better agreement with the exact calculations for planar waves, it is plausible that the agreement for the elastic case would be in better agreement for spherical waves. Thus, it is plausible that the RAVS calculations for spherical waves would be almost the same as the exact calculations. This is important because spherical waves are of much more practical interest than planar waves.

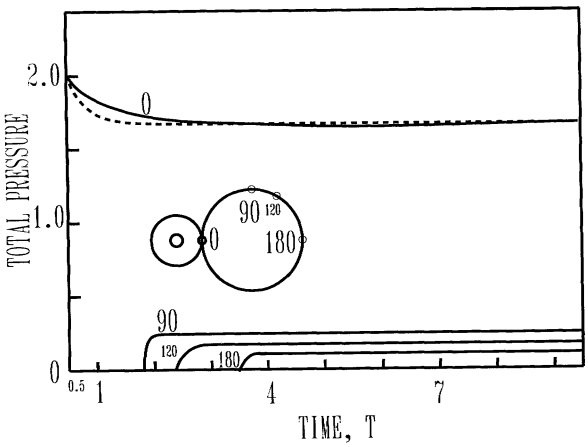

FIGURE 8 Rigid cylinder attacked by a spherical wave with constant pressure; nearest distance = $0.5a_1$, longitudinal distance = 0.

SUMMARY AND CONCLUSIONS

An equation of motion for a structural surface was presented. The equations for the pressure that develops when an acoustic wave interacts with a curved and compliant surface were also presented. These equations were derived using the RAVS model (see Waldo, 1994). With these equations, an expression for the velocity of the structural surface was derived from the equation of motion. A numerical method was presented for using this

expression. This was applied to the case of a planar wave attacking an elastic cylindrical shell. Calculations that were made from a computer program, using the RAVS model, were shown to be in good agreement with all of the exact calculations presentd by Huang (1970) for all locations and times. Thus, it is concluded that the RAVS model gives a good approximation for an elastic cylinder being attacked by a planar wave. The RAVS approximation becomes even better for spherical attacking waves that are of much more practical interest (Waldo, 1994). In these situations, the *source* of the attacking wave is a *finite* distance from the structural surface. In the limit of the soruce being very close to a structural surface, the structural surface can be considered as planar. In this situation, the RAVS approximation becomes exact for a rigid surface and a free surface. Of course, the results of the RAVS model should be compared to other exact calculations such as those for an elastic spherical shell (see Huang, 1969).

APPENDIX: SOLUTION OF EQUATION OF MOTION

Substituting p_{rad} from Eq. (16) into Eq. (2) and the resulting expression into the equation of motion, Eq. (1), gives

$$m\dot{u}(t) = p_{\text{hydro}} + p(t) + p_{\text{scat}}(t) - e^{-(ct/b)} \int_{-r/c}^{t} e^{ct'/b} \frac{\rho c \dot{u}(t')}{\cos \beta} dt' - p_{\text{str}}(t). \tag{A.1}$$

Multiplying both sides of this equation by exp (ct/b), differentiating both sides of the resulting equation with respect to t, and solving the differential equation gives

$$m\dot{u}(t) = \dot{I}(t) + \frac{c}{b} I(t) + \dot{I}_{\text{scat}}(t) + \frac{c}{b} I_{\text{scat}}(t) - \dot{I}_{\text{str}}(t) - \frac{c}{b} I_{\text{str}}(t), \tag{A.2}$$

where

$$I(t) = e^{-\eta t} \int_0^t e^{\eta t'} p(t')\, dt',$$

$$I_{\text{scat}}(t) = e^{-\eta t} \int_0^t e^{-\eta t'} p_{\text{scat}}(t')\, dt'. \tag{A.3}$$

$$I_{\text{str}}(t) = e^{-\eta t} \int_{-r/c}^{t} e^{\eta t'} [p_{\text{str}}(t') - p_{\text{hydro}}]\, dt', \tag{A.4}$$

and

$$\eta = \frac{c}{b} + \frac{\rho c}{m \cos \beta} \tag{A.5}$$

is called "the damping coefficient." The lower limit of the intergration in Eq. (A.3) is zero because the pressure of the attacking wave and, thus, the pressure of the scattered wave are zero before their arrival at $t = 0$.

Equation (13) shows that

$$\dot{p}_{\text{scat}}(t) + \frac{c}{b} p_{\text{scat}}(t) = \left[\dot{p}(t) + \frac{c}{r} p(t)\right] \frac{\cos \theta}{\cos \beta}. \tag{A.6}$$

By performing the integration,

$$e^{-\eta t} \int_0^t e^{-\eta t'} (\ )\, dt' \tag{A.7}$$

on all of the terms in Eq. (A.6), it is seen that

$$\begin{aligned} & e^{-\eta t} \int_0^t e^{\eta t'} \dot{p}_{\text{scat}}(t')\, dt' \\ & + e^{-\eta t} \int_0^t e^{\eta t'} \frac{c}{b} p_{\text{scat}}(t')\, dt' \\ & = \left[e^{-\eta t} \int_0^t e^{\eta t'} \dot{p}(t')\, dt' \right. \\ & \left. + e^{-\eta t} \int_0^t e^{\eta t'} \frac{c}{r} p(t')\, dt' \right] \frac{\cos \theta}{\cos \beta}. \end{aligned} \tag{A.8}$$

By integrating by parts, it is seen that

$$\begin{aligned} & e^{-\eta t} \int_0^t e^{\eta t'} \dot{\boldsymbol{p}}_{\text{scat}}(t')\, dt' \\ & = p_{\text{scat}}(t) - \eta e^{-\eta t} \int_0^t e^{\eta t'} \boldsymbol{p}_{\text{scat}}(t')\, dt' \\ & = \frac{d}{dt} \left[e^{-\eta t} \int_0^t e^{\eta t'} \boldsymbol{p}_{\text{scat}}(t')\, dt' \right]. \end{aligned} \tag{A.9}$$

This demonstrates that the operation of Eq. (A.7) on the derivative of a function equals the derivative of the operation of Eq. (A.7) on that function. It is noted that the pressure of the attacking wave, and thus, the pressure of the scattered wave, is zero in the limit of positive time going to zero. If there is a sudden rise in the pressure at time zero, this can be represented to any desired accuracy

by a function that is zero in the limit of positive time going to zero. The function would then increase at an arbitrarily high rate of change up to its first peak pressure. Thus, Eq. (A.8) is the same as

$$\begin{aligned}&\frac{d}{dt}\left[e^{-\eta t}\int_0^t e^{\eta t'}\,p_{\text{scat}}(t')\,dt'\right]\\&+\frac{c}{b}e^{-\eta t}\int_0^t e^{\eta t'}\,p_{\text{scat}}(t')\,dt'\\&=\left\{\frac{d}{dt}\left[e^{-\eta t}\int_0^t e^{\eta t'}\,p(t')\,dt'\right]\right.\\&\left.+\frac{c}{r}e^{-\eta t}\int_0^t e^{\eta t'}\,p(t')\,dt'\right\}\frac{\cos\boldsymbol{\theta}}{\cos\boldsymbol{\beta}}.\end{aligned}\tag{A.10}$$

By substituting Eq. (A.3), this becomes

$$\dot{I}_{\text{scat}}(t)+\frac{c}{b}I_{\text{scat}}(t)=\left[\dot{I}(t)+\frac{c}{r}I(t)\right]\frac{\cos\boldsymbol{\theta}}{\cos\boldsymbol{\beta}}.\tag{A.11}$$

Substituting Eq. (A.11) into Eq. (A.2) gives an equivalent equation of motion,

$$\begin{aligned}m\dot{u}(t)=\dot{I}(t)+\frac{c}{b}I(t)+\left[\dot{I}(t)+\frac{c}{r}I(t)\right]\frac{\cos\boldsymbol{\theta}}{\cos\boldsymbol{\beta}}\\-\dot{I}_{\text{str}}(t)-\frac{c}{b}I_{\text{str}}(t),\end{aligned}\tag{A.12}$$

where $I(t)$ and $I_{\text{str}}(t)$ are determined by Eqs. (A.3) and (A.4). The right-hand side of Eq. (A.12) does not involve the (unknown) velocity [as in Eq. (A.1)]. However, the right-hand side does require the mass density of the structural surface and the structural resistance pressure. Integration of both sides of Eq. (A.12) and dividing both sides of the resulting expression by m gives the velocity of the structural surface,

$$\begin{aligned}u(t)=&\frac{I(t)}{m}\left(1+\frac{\cos\boldsymbol{\theta}}{\cos\boldsymbol{\beta}}\right)\\&+\frac{1}{m}\left(\frac{c}{b}+\frac{c}{r}\frac{\cos\boldsymbol{\theta}}{\cos\boldsymbol{\beta}}\right)\left[\frac{1}{\boldsymbol{\eta}}\int_0^t p(t')\,dt'-\frac{I(t)}{\boldsymbol{\eta}}\right]\\&-\frac{I_{\text{str}}(t)}{m}\\&-\frac{c}{mb}\left\{\frac{1}{\boldsymbol{\eta}}\int_{-r/c}^t\left[p_{\text{str}}(t')-p_{\text{hydro}}\right]dt'-\frac{I_{\text{str}}(t)}{\boldsymbol{\eta}}\right\}.\end{aligned}\tag{A.13}$$

REFERENCES

Cole, R. H., 1948, *Underwater Explosions,* Dover Publications, Inc., New York.

Huang, H., 1969, "Transient Interaction of Plane Acoustic Waves with a Spherical Elastic Shell," *Journal of the Acoustical Society of America,* Vol. 45, pp. 661–670.

Huang, H., 1970, "An Exact Analysis of the Transient Interaction of Acoustic Plane Waves with a Cylindrical Elastic Shell," *Journal of Applied Mechanics,* Vol. 37, pp. 1091–1099.

Huang, H., 1975, "Scattering of Spherical Pressure Pulses by a Hard Cylinder," *Journal of the Acoustical Society of America,* Vol. 58, pp. 310–317.

Jenkins, F. A., and White, H. E., 1957, *Fundamentals of Optics,* 3rd ed., McGraw–Hill, New York.

Waldo, G. V., Jr., "An Approximate Model for the Pressure That Develops When an Acoustic Wave Interacts with a Curved and Compliant Surface," in *Proceedings of the 65th Shock and Vibration Symposium,* Vol. II, 1994, Shock and Vibration Information Analysis Center, Arlington, VA, pp. 185–198.

Waldo, G. V., Jr., "Comparison of the Virtual-Source Model to Exact Calculations," in *Proceedings of the 66th Shock and Vibration Symposium,* Vol. I, 1995, Shock and Vibration Information Analysis Center, Arlington, VA, pp. 153–163.

Waldo, G. V., Jr., 1996, "*R*eflected-*A*fterflow *V*irtual-*S*ource (RAVS) Model Response Compared to Exact Calculations for Elastic Cylinders Attacked by Planar Waves," National Technical Information Service, AD No. A306110.

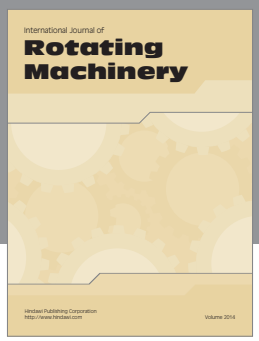

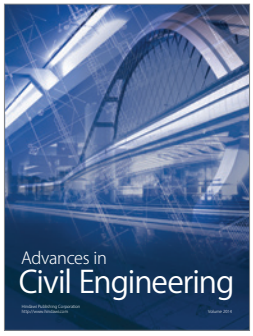

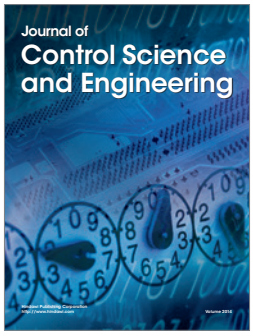

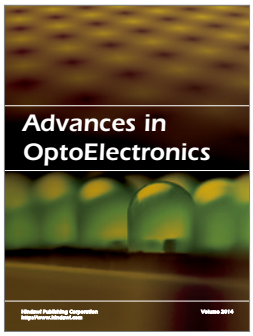

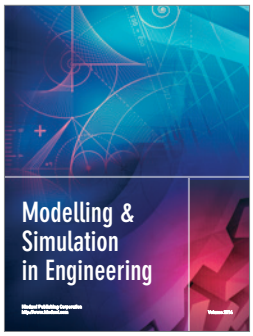

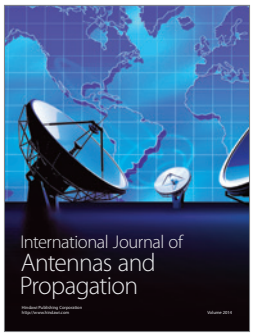

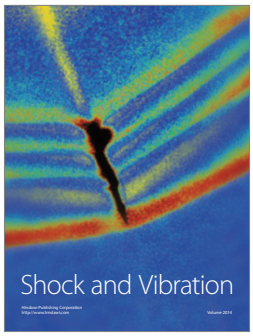

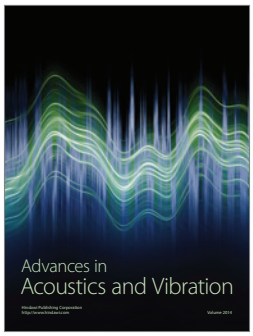

Hindawi

Submit your manuscripts at
http://www.hindawi.com